J Mol Model (2009) 15:1165–1173
DOI 10.1007/s00894-009-0467-4

ORIGINAL PAPER

# Theoretical study on the series of $[Au_3Cl_3M_2]$ complexes, with M = Li, Na, K, Rb, Cs

**Jesús Muñiz · Luis Enrique Sansores · Pekka Pyykkö · Ana Martínez · Roberto Salcedo**

Received: 24 November 2008 / Accepted: 12 January 2009 / Published online: 26 February 2009


**Abstract** The prediction of the series of complexes $[Au_3Cl_3M_2]$ with M = Li, Na, K, Rb and Cs, has been achieved at the ab initio level of theory. All geometries were fully optimized at the MP2 level of theory; the central $Au_3$ cluster is capped by chlorine atoms and the alkaline metals lie above and below the plane of the central ring; aurophilic interactions were found on the metal cluster, and also a strong aromatic character coming from the delocalized d-electrons of the Au atoms according to nuclear independent chemical shift calculations. On the other hand, the chemical hardness parameter was used to test the stability of the series of complexes, and the Fukui indexes of electrophilic and nucleophilic attack were employed to explore possible sites where chemical reactivity may play a role.

**Keywords** Aurophilic interactions · Aromaticity · Reactivity · Ab initio calculations

## Introduction

The quest for transition metal monolayer sheet complexes capped by ligands in sandwich-like structures [1] has entered a new field in the discovery of novel species since the synthesis of the sandwich Pd compounds $[Pd_3(C_7H_7)_2Cl_3]$ [PPh] and $[Pd_5(naphthacene)_2\ (toluene)]$ $[B(Ar_f)_4]_2$ (4-toluene)], with B $(Ar_f)_4 = B[3,5(CF_3)_2C_6H_3]_4$. Structures such as $Ni_3(benzene)_2$ have also been observed in $Ni_n(benzene)_m$ clusters [2]. The importance of the study of this type of complex is their use as building blocks in larger systems where unsaturated hydrocarbons are adsorbed on metallic surfaces. In addition, their potential uses in catalysis, as Pd clusters, is of great interest due to the large range of applications [1].

Several theoretical studies on the existence and stability of sandwich monolayer sheet compounds with transition metal atoms have been performed at the extended Hückel level [3]. More recently, the search has been extended to the prediction of the Au cluster $[Au_3Cl_3Tr_2]^{2+}$, where a trigold monolayer sheet capped by chlorines and sandwiched by two cycloheptatrienyl ($Tr^+$) ligands has been studied at the ab initio and density functional theory (DFT) levels [4]. The bonding of the Tr ligands to the Au cluster appears to be dominated by an electronic back-donation interaction to the bonding region from the trigold complex to the Tr ligands. The bonding in the $[Au_3Cl_3]$ monolayer sheet was ruled by a d–d orbital interaction mixed with a σ-character from the Au 6s orbitals. Furthermore, Au–Au interactions were attributed to a strong aurophilic bonding: aurophilicity is a term first introduced by Schmidbaur [5], referring to a contraction in Au–Au bond distances. The bond lengths are typically in the range 300–360 pm. Some cases where Au–Au interactions are less than 300 pm have also been reported [6]. The energy of the aurophilic interaction is characterized to be at the order of magnitude of the weakest covalent bonds and the strongest hydrogen bonds; i.e. at a widely known interaction energy ranging from 5 to 15 kcal $mol^{-1}$ [7–10]. Theoretical studies have shown that the predominant mechanism behind the interaction is dispersion.

It has been shown that the stability of the complex $[Au_3Cl_3Tr_2]^{2+}$ can be attributed to the strong aurophilic

J. Muñiz (✉) · L. E. Sansores · A. Martínez · R. Salcedo
Instituto de Investigaciones en Materiales,
Universidad Nacional Autónoma de México,
Apartado Postal 70-360, México, DF 04510, Mexico
e-mail: jesus@iim.unam.mx

P. Pyykkö
Department of Chemistry, University of Helsinki,
P.O.B. 55 (A.I. Virtasen aukio 1), 00014 Helsinki, Finland

bonding found in the metal monolayer sheet and the aromatic character observed in the trigold compound and Tr ligands attached to it. Examples of the aromaticity of coinage metal clusters have been reported recently by Tsipis et al. [11, 12] in a theoretical study performed at the DFT level: the series $M_4H_4$ (with M = Cu, Ag, Au) was predicted to be stable, with $D_{4h}$ symmetry and a weak aromatic character; the Cu and Ag congeners have the same nuclear independent chemical shift (NICS) value, while in the $Au_4H_4$ species, the aromaticity is greater. On the other hand, compounds of the type $[M_4Li_2]$, with M = Cu, Ag and Au, were also predicted at the DFT level [13]. The metal ring compounds have $D_{4h}$ symmetry and, in every species, the Li atoms are flanked above and below the plane of the ring; this series of complexes shows a clear aromatic behavior that also occurs in the Ag and Cu species, and is greater in the $Au_4Li_2$ compound. Wannere et al. [13] found, by using NICS calculations, that these series of complexes are the first examples where "δ-aromaticity" is present; i.e., an aromatic character where the delocalized d-electrons are the main mechanism behind the observed aromaticity. It was shown that the participation of the $d_z^2$ and $d_{x^2-y^2}$ orbitals of the metal atoms dominate the phenomenon. Species of the form $[M_4Li]^-$ and $[M_4Na]^-$ have also been predicted at the MP2 (second order Møller-Plesset perturbation theory) and CCSD(T) (coupled cluster calculation with single and double substitutions with noniterative triple excitations) levels of theory [14]. The latter series of compounds have not been shown to possess catalytic properties. The group of Au ring complexes showing an aromatic character is very limited, and the possible reactivity properties of this kind of compound have not been explored. The aim of the present work is to study the existence and stability of novel Au ring compounds and to determine possible reactive sites.

## Computational methods

All geometry optimizations were performed with the MP2 [15] computational method, which explicitly accounts for dispersion effects—important in the description of aurophilic interactions. The Stuttgart small-core pseudorelativistic effective core potential [16] with 19 valence electrons was employed for gold. The effective core potential (ECP) was used with the valence triple-ζ plus one polarization type; i.e., the basis set TZVP, which is an optimized contracted Gaussian basis set computed by Schäfer et al. [17]. Two additional f-type polarization functions calculated by Pyykkö et al. [18] were augmented to the basis set ($\alpha_f$=0.2, 1.19). The first function is a diffuse f orbital necessary for the intermolecular interaction, while the second is a polarization function important for describing the covalent bonding involving the Au $d^{10}$ shell. For the non-Au atoms (Li, Na, K), the 6-31++G(2df, p) basis set was used [19, 20]; while for Rb and Cs atoms, the LANL2DZ [21] small-core pseudopotential with 19 valence electrons was used, which also includes relativistic effects.

Electrostatic and bonding energies were evaluated using the methodology developed by Ziegler et al. [22, 23] based on DFT. Slater's Xα exchange potential [24, 25] was used (with α=0.7). The Dirac method [26] was employed to compute the atomic core orbitals, which were maintained unrelaxed in the series of complexes. To reduce the computational cost, the inner core shells were fixed; the shell $[1s^2–2p^6]$ was frozen for Cl, $[1s^2–4d^{10}]$ for Au and $[1s^2]$, $[1s^2]$, $[1s^2–2p^6]$, $[1s^2–3d^{10}]$ and $[1s^2–4d^{10}]$ for Li, Na, K, Rb and Cs, respectively. The scalar relativistic zero-order relativistic approximation (ZORA) was applied in the DFT calculations [27–29], since the relativistic effects play an important role in systems where aurophilic interactions are present. DFT computations were carried out with the high quality triple-ζ plus one polarization basis set, which is a Slater-type basis (STO-TZP).

The aromaticity in the series of complexes was studied by NICS methodology as given by Schleyer et al. [30]. To test the stability of the molecules presented in this work, the chemical potential μ [31] and chemical hardness η [32] from DFT were used, which are defined as:

$$\mu = \left(\frac{\partial E}{\partial N}\right)_{T,v(r)} \tag{1}$$

and

$$\eta = \frac{1}{2}\left(\frac{\partial^2 E}{\partial N^2}\right)_{T,v(r)} \tag{2}$$

where $E$ is the total energy, $N$ is the total number of electrons in the system, $T$ corresponds to temperature and $\upsilon(r)$ is the external potential. We applied the well known finite-difference approximation to evaluate μ and η, considering that $E$ varies quadratically with respect to the number of electrons. Consequently, these parameters [33] may be given in orbital grounds as:

$$\mu = -\left(\frac{IP + AE}{2}\right) \tag{3}$$

$$\eta = \left(\frac{IP - AE}{2}\right) \tag{4}$$

where $IP$ is the ionization potential and $AE$ is the electron affinity. These two quantities can also be defined based on orbitals, on the basis of Koopmans' theorem as $IP = -E_{HOMO}$ and $AE = -E_{LUMO}$, where $E_{HOMO}$ and $E_{LUMO}$ are the energies of the highest occupied molecular orbital (HOMO)

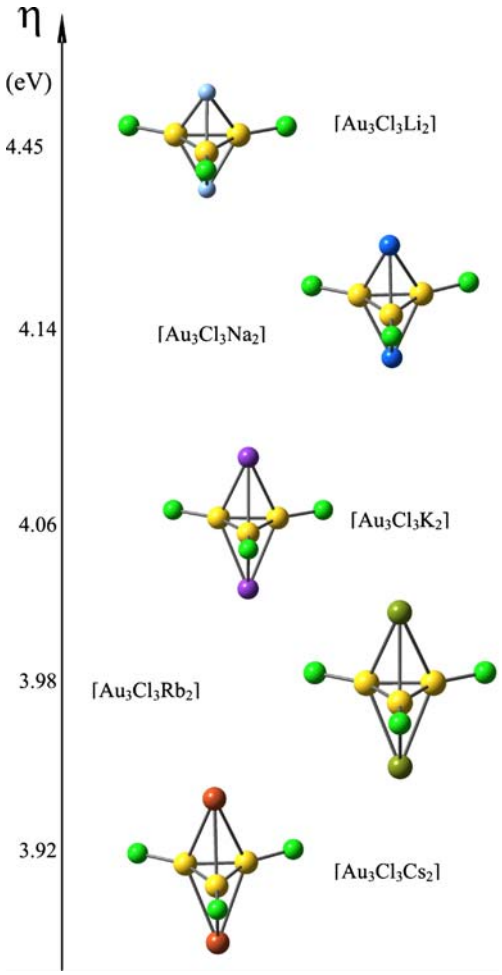


**Fig. 1** Molecular representations of the series of complexes $[Au_3Cl_3M_2]$ (M = Li, Na, K, Rb, Cs) and their corresponding chemical hardness

and lowest unoccupied molecular orbital (LUMO), respectively (considering that this orbital approach may introduce a small error that is not significant with respect to the overall calculation). In addition, to test probable reactive sites in the series of compounds, the Fukui local functions for electrophilic and nucleophilic agents were determined in a finite-difference basis by the gross natural charge ($q$) at site $k$, where $k$ represents an atom in the molecule with N−1 and N+1 electrons. The Fukui index for electrophilic and nucleophilic attacks are given by:

$$f_k^- = q_k(N) - q_k(N-1) \tag{5}$$

and

$$f_k^+ = q_k(N+1) - q_k(N), \tag{6}$$

respectively [34].

The aurophilic interaction was studied as stated by the Herschbach and Laurie relation [10]:

$$R_{Au-Au} = 268pm + 29 \cdot \ln([N/cm]/k_{Au-Au}) \tag{7}$$

where $R_{Au-Au}$ corresponds to the equilibrium Au–Au distance (given in picometers) and $k_{Au-Au}$ represents the force constant in N/cm. The calculations were performed using the GAUSSIAN03 [35] code and the ZORA computations were carried out with the Amsterdam Density Functional (ADF) package [36, 37].

## Results and discussion

### Structural description

Full geometry optimizations were carried out at the ab initio level for the series of complexes $[Au_3Cl_3M_2]$; where M corresponds to the alkaline metals M = Li, Na, K, Rb and Cs. The molecular structures are shown in Fig. 1 and the structural parameters are presented in Table 1. In the series of complexes, the $M^+$ lies above and below the $[Au_3Cl_3]^{2-}$ monolayer sheet and is bonded to the metal cluster since the $M^+$ cations provide a natural positive charge ranging from +0.894 to +0.980, increasing down the alkali metal group (see Table 2), which indicates that the $[Au_3Cl_3]^{2-}$ cluster attracts the $M^+$ cations electrostatically. All structures belong to the $D_{3h}$ point group, except the $[Au_3Cl_3Cs_2]$ species, which distorts to the $C_{3h}$ point group. The bond length from the $Au_3Cl_3$ plane to the alkaline metal increases

**Table 1** Main bond lengths of the series of complexes $[Au_3Cl_3M_2]$. The quantities in parenthesis correspond to the optimized parameters at the Hartree-Fock (HF) level. *MP2* Second order Møller-Plesset perturbation theory, *SCF* self-consistent field

| | Computational method | | | | |
|---|---|---|---|---|---|
| | MP2 (SCF) | | | | |
| Bond (pm) | $[Au_3Cl_3Li_2]$ | $[Au_3Cl_3Na_2]$ | $[Au_3Cl_3K_2]$ | $[Au_3Cl_3Rb_2]$ | $[Au_3Cl_3Cs_2]$ |
| Au–Au | 265.0(279.1) | 263.4(277.7) | 262.4(276.0) | 262.0(276.0) | 261.7(275.8) |
| Au–Cl | 230.4(238.7) | 232.0(240.8) | 233.7(243.1) | 234.0(243.8) | 234.5(244.7) |
| $Au_3$–M | 217.5(221.0) | 259.4(263.4) | 309.3(314.8) | 325.0(339.1) | 345.0(360.7) |
| Point group[a] | $D_{3h}$ | $D_{3h}$ | $D_{3h}$ | $D_{3h}$ | $C_{3h}(D_{3h})$ |

[a] The point groups are the same at both levels, except for the $[Au_3Cl_3Cs_2]$ species

**Table 2** Natural charges in the series of complexes $[Au_3Cl_3M_2]$

| | $[Au_3Cl_3Li_2]$ | $[Au_3Cl_3Na_2]$ | $[Au_3Cl_3K_2]$ | $[Au_3Cl_3Rb_2]$ | $[Au_3Cl_3Cs_2]$ |
|---|---|---|---|---|---|
| Au | 0.01 | 0.01 | 0.02 | 0.02 | 0.03 |
| Cl | −0.60 | −0.63 | −0.67 | −0.67 | −0.68 |
| M | 0.89 | 0.93 | 0.97 | 0.97 | 0.98 |

down the group, while the Au–Cl length is kept in the 230–234 pm range

The Au–Au bond length in the $[Au_3Cl_3Li_2]$ compound is 265 pm, which presumably corresponds to an aurophilic interaction; this is an unusually short Au–Au distance, since aurophilic bonding commonly ranges from 275 to 344 pm [6]. By comparison, an Au–Au distance of 282 pm has been previously reported [38] in the bare $Au_3$ cluster, and a bond length of about 270 pm and 282 pm in the gold monolayer sheet (the species is not symmetric) reported in the analogue $[Au_3Cl_3Tr_2]^{2+}$ compound [4].

A rough measure of the aurophilic attraction can be obtained by comparing the results at the SCF and MP2 levels (see Table 1): a shortening of the Au–Au distance of about 14 pm is observed. This suggests an important Au–Au interaction. Wiberg bond orders of about 0.3 were also calculated. Note, however, that the dispersion interactions do not require any orbital overlap. Eventual covalent contributions may exist independently. For the latter, see the spatial representation (Fig. 2) of the frontier molecular orbitals: the HOMO is composed of the Cl p orbitals and the main contribution is located at the center of the ring formed by the Au 6s orbitals. On the other hand, the HOMO-1 and HOMO-2 are made of the $d_{xy}$ and $d_{xz}$ orbitals of the gold atoms, which can clearly be seen as a d–d interaction, with a mixture of the s orbitals. Furthermore, the HOMO-9 is a bonding orbital with a large contribution coming from the Au 6s orbitals (see Fig. 2), and corresponds to the HOMO of the formal $Au_3^{3+}$ moiety [4]. This is corroborated by the gross population analysis presented in Table 3 for the Au atoms of each species of the series, where a large s population is observed, consistent with the s orbital contribution on the HOMO. The total d orbital population, which is smaller than 10e, reveals the breaking of the $5d^{10}$ electronic structure that leads to the formation of the d–d bonding with a participation of the s–s interaction. The latter is also consistent with the electronic configuration of the gold atoms through the series $[Au_3Cl_3M_2]$ as shown in Table 4. Briefly, this is a further example of the facile 5d–6s hybridization of gold. The LUMO in the series of complexes is a combination of the outer s and p orbitals of Au and alkaline atoms, with slight $3p_z$ orbital contributions coming from the chlorine atoms (see Fig. 2).

A vibrational analysis was performed in the series of complexes, and no imaginary frequencies were found. The force constants from these calculations are typical of the aurophilic range, when compared with the empirical relation of Herschbach and Laurie [10], where the Au–Au bond distance (in pm) and the force constants (in N/cm) are both involved; this relationship (see Eq. 7) is valid in the range 247–355 pm. The Au–Au vibrational modes ($\nu_{Au-Au}$) and the Au–Au bond lengths calculated from Eq. 7 are reported in Table 5; the computed Au–Au modes appear to be stronger than those found in other systems with aurophilic interactions [39]. These results are in reasonable agreement with the values obtained on the ground state geometry of the series of compounds, indicating that an aurophilic bonding is formed.

## Stability of the series of compounds

According to the DFT, and also from empirical observation, the most stable species in a group of similar systems is the one with the greatest chemical hardness—this is called "*the principle of chemical hardness*" [40–44]. The hardness is

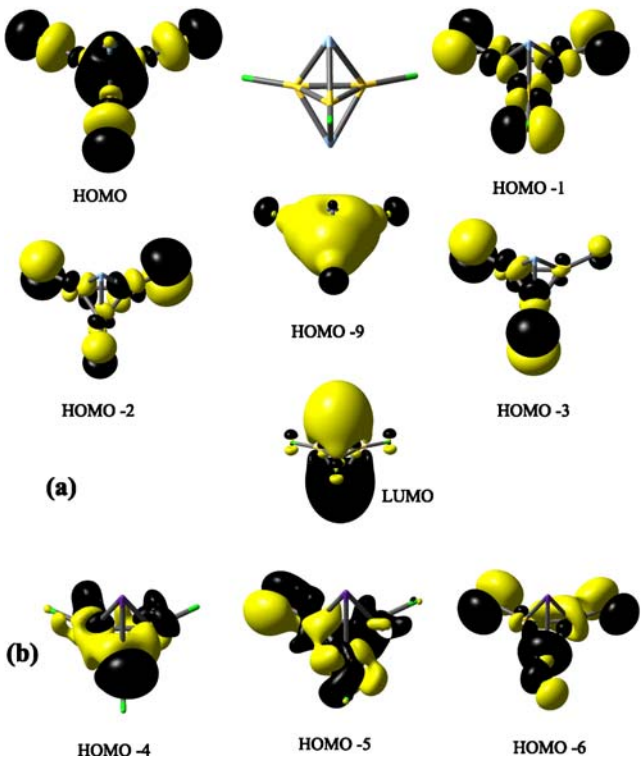


**Fig. 2** **a** $[Au_3Cl_3Li_2]$ Hartree-Fock (HF) frontier molecular orbitals (MOs). Note that the whole series present the same spatial representations. **b** $[Au_3Cl_3Rb_2]$ lower energy MOs

**Table 3** Natural bond orbital (NBO) population analysis for the series of complexes $[Au_3Cl_3M_2]$

| | NBO population analysis | | | | | | | | | | | | | | |
|---|---|---|---|---|---|---|---|---|---|---|---|---|---|---|---|
| | Charge population of $[Au_3Cl_3Li_2]$ | | | Charge population of $[Au_3Cl_3Na_2]$ | | | Charge population of $[Au_3Cl_3K_2]$ | | | Charge population of $[Au_3Cl_3Rb_2]$ | | | Charge population of $[Au_3Cl_3Cs_2]$ | | |
| | Au1 | Au2 | Au3 | Au1 | Au2 | Au3 | Au1 | Au2 | Au3 | 3.101 | 3.101 | 3.101 | Au1 | Au2 | Au3 |
| S | 3.119 | 3.116 | 3.117 | 3.105 | 3.105 | 3.105 | 3.105 | 3.105 | 3.105 | 2.016 | 2.016 | 2.030 | 3.099 | 3.099 | 3.099 |
| $p_x$ | 2.020 | 2.019 | 2.037 | 2.018 | 2.018 | 2.038 | 2.017 | 2.017 | 2.032 | 2.016 | 2.016 | 2.016 | 2.016 | 2.016 | 2.030 |
| $p_y$ | 2.020 | 2.020 | 2.020 | 2.022 | 2.021 | 2.022 | 2.018 | 2.018 | 2.018 | 2.025 | 2.025 | 2.011 | 2.015 | 2.015 | 2.015 |
| $p_z$ | 2.032 | 2.031 | 2.014 | 2.031 | 2.031 | 2.012 | 2.027 | 2.027 | 2.011 | 1.998 | 1.998 | 1.994 | 2.025 | 2.025 | 2.011 |
| $d_{xy}$ | 1.995 | 1.995 | 1.984 | 1.996 | 1.996 | 1.988 | 1.998 | 1.998 | 1.993 | 1.923 | 1.923 | 1.962 | 1.998 | 1.998 | 1.995 |
| $d_{xz}$ | 1.926 | 1.925 | 1.958 | 1.925 | 1.925 | 1.961 | 1.923 | 1.923 | 1.962 | 1.995 | 1.995 | 1.999 | 1.923 | 1.923 | 1.962 |
| $d_{yz}$ | 1.988 | 1.988 | 1.998 | 1.991 | 1.991 | 1.999 | 1.995 | 1.995 | 1.999 | 1.977 | 1.977 | 1.881 | 1.996 | 1.996 | 1.999 |
| $d_{x^2-y^2}$ | 1.972 | 1.972 | 1.873 | 1.975 | 1.975 | 1.878 | 1.977 | 1.977 | 1.879 | 1.920 | 1.920 | 1.978 | 1.978 | 1.978 | 1.881 |
| $d_{z^2}$ | 1.915 | 1.915 | 1.981 | 1.918 | 1.919 | 1.980 | 1.919 | 1.919 | 1.979 | 3.101 | 3.101 | 3.101 | 1.920 | 1.920 | 1.978 |

obtained from DFT parameters (see Eq. 4); nevertheless, the ionization energy and electron affinity computed at the ab initio level are better than those at the DFT level, since it is known that, in calculations performed with DFT, the electronic density decays faster than at the ab initio level, producing a gradient with higher density. Taking the latter into account, the ab initio MP2 level was used to calculate the chemical hardness of the species under study. The hardness was computed from Eq. 4, along with the ionization potentials and electron affinities calculated from Koopmans' theorem.

It was found that the $[Au_3Cl_3Li_2]$ species presents the greatest hardness of the group (see Table 6 and Fig. 1), and it can thus be stated that this system is the most stable of the series. The $[Au_3Cl_3Na_2]$ and $[Au_3Cl_3K_2]$ analogues have lower hardness. Finally, the $[Au_3Cl_3Rb_2]$ and $[Au_3Cl_3Cs_2]$ species present the lowest chemical hardness. All chemical hardness were comparable, indicating a comparable chemical stability for these species.

## Reactivity

The reactivity of molecules has been studied widely using Fukui functions [33]. In this work, we calculated the Fukui indices of electrophilicity ($f^-$) and nucleophilicity ($f^+$) as given by the finite difference approximation (Eqs. 5 and 6, respectively). These indices represent local parameters that provide an insight into the possible sites in a molecule where reactivity may be present, playing a role as an electrophilic attack (given by $f^-$) or as nucleophilic attack (as stated by $f^+$). The calculations of the Fukui indices were performed in accordance with the NBO scheme [45], the results are presented in Table 7. The electrophilic index in the gold atoms in each of the species of the series reaches a maximum at $[Au_3Cl_3Cs_2]$, while the values for $[Au_3Cl_3K_2]$ and $[Au_3Cl_3Rb_2]$ are comparable. For comparison, the values of the electrophilic indices of reactivity were computed for the gold atoms in the naked $Au_3$ molecule as 0.17 and 0.33, for the neutral (at the MP2/LANL2DZ level) and cationic (at the MP2/TZVP level) systems, respectively. The naked $Au_3$ compound has been shown to play a role in absorption mechanisms [46, 47] and, according to the latter results, the $[Au_3Cl_3M_2]$ series of complexes may present analogous properties. This indicates that an acid-catalyzed reaction may take place via electrophilic attack at the gold atoms of the series. This may be achieved, for instance, by carbon or nitrogen atoms belonging to carbon monoxide or nitrogen monoxide molecules, respectively. Both are examples of environmental contaminant agents [39]. The latter is feasible since the natural charges (at the MP2 level) on carbon and nitrogen atoms in CO and NO molecules are +0.616 and +0.318, respectively. Taking into account the chemical hardness analysis reported previously on the stability of the species and the Fukui indices reported in Table 6, the best candidates for absorbing CO or NO molecules may be compounds $[Au_3Cl_3Na_2]$, $[Au_3Cl_3Rb_2]$ or $[Au_3Cl_3K_2]$, since these species are the most stable of the series and

**Table 4** Electronic configuration of Au atoms for the series of $[Au_3Cl_3M_2]$ species according to the NBO method

| | $[Au_3Cl_3Li_2]$ | $[Au_3Cl_3Na_2]$ | $[Au_3Cl_3K_2]$ | $[Au_3Cl_3Rb_2]$ | $[Au_3Cl_3Cs_2]$ |
|---|---|---|---|---|---|
| Au electronic Configuration | $5d^{9.79}6s^{1.12}$ $6p^{0.07}5f^{0.01}$ | $5d^{9.80}6s^{1.10}$ $6p^{0.07}5f^{0.01}$ | $5d^{9.81}6s^{1.10}$ $6p^{0.06}$ | $5d^{9.81}6s^{1.10}$ $6p^{0.06}$ | $5d^{9.62}6s^{1.09}$ $6p^{0.10}5f^{0.10}$ |

**Table 5** Au–Au stretching frequencies ($\nu_{Au\text{-}Au}$), force constants ($k_{Au\text{-}Au}$) and estimated Au–Au bond lengths

| | Au–Au stretching ($cm^{-1}$) frequency ($\nu_{Au\text{-}Au}$) | $k_{Au-Au}$(N/cm) | $R_{Au-Au}$(pm) | Calculated MP2 Au–Au bond length (pm) |
|---|---|---|---|---|
| $[Au_3Cl_3Li_2]$ | 166.6(A′) | 1.42 | 258.0 | 265.0 |
| $[Au_3Cl_3Na_2]$ | 163.0($A_1$) | 0.73 | 277.2 | 263.4 |
| $[Au_3Cl_3K_2]$ | 174.8( A′) | 1.67 | 253.2 | 262.4 |
| $[Au_3Cl_3Rb_2]$ | 174.3( A′) | 1.70 | 252.6 | 262.0 |
| $[Au_3Cl_3Cs_2]$ | 175.0( A′) | 1.70 | 252.7 | 261.7 |

possess the largest $f^-$ indexes. Although CO and NO adsorption on Au clusters has been explored widely on theoretical grounds [48], and the synthesis of Au clusters of less than six atoms has not been achieved [49], the series of complexes reported in this work might represent a new route to reach this goal.

The electrophilic indices with negative signs obtained for the Cl atoms are artifacts of the methodology and do not have a physical significance. On the other hand, the nucleophilic indices on the series of complexes are greatest on the $M^+$ cations (M = Li, Na, K, Rb, Cs), which suggests that a reaction on those sites might take place by protonation. According to the results for $f^+$ indexes on the Au and Cl atoms, nucleophilic attack on these sites is less probable.

## Donation and back-donation interactions

A charge decomposition analysis (CDA) was performed [50] on the ground state geometries; this study depicts the donor–acceptor interactions, partitioning the molecule to be studied into two fragments. The methodology consists of building the wave functions of the compounds; the linear combination of the donor and acceptor fragment orbitals (LCFO) is then taken into account. The CDA study gives the charge donation from the occupied orbitals of the donors to the unoccupied orbitals of the acceptor; a back-donation from the occupied orbitals of the acceptor to the virtual orbitals of the donor is also returned and, finally, the repulsive polarization contribution quantifies the charge removed from the overlapping area of the occupied orbitals of the donor and acceptor fragments. According to the CDA study, the donation interaction is virtually negligible, since −11.5, −5.7, −14.5, −7.7 and −12.6e is returned, for species **1–5**, respectively; this means that no electronic charge is donated to the bonding region. Nevertheless, a slight back-donation interaction is observed from the $[Au_3Cl_3]^{2-}$ cluster to the $2M^+$ cations: +0.60, +0.16, +0.06, +0.30 and +0.34e are back-donated on compounds **1–5**, respectively, from the trigold complex to the bonding region. The molecular orbitals mainly involved in the back-donating character are HOMO-12, HOMO-16, HOMO, HOMO-20 and HOMO-23 for compounds **1–5**, respectively. The contour plots for these MOs, which lie in the perpendicular direction to the plane of the trigold complex, are depicted in Fig. 3. The orbital character in the bonding between the $[Au_3Cl_3]^{2-}$ monolayer sheet and the $2M^+$ (M = Li, Na, K, Rb, Cs) cations is small as observed from the CDA study since, as stated, this interaction is governed mainly by the electrostatic attraction among the $M^+$ cations and the gold cluster.

## Bonding energies

The total bonding energy of the series of compounds was studied using the methodology of Ziegler et al. [22, 23] at the DFT/X Alpha//MP2 level of theory. In this method, the total interaction energy is split into three contributions, namely, the Pauli repulsion energy, the electrostatic attraction and the orbital relaxation. The first contribution ($E_{Pauli}$) is the increase in kinetic energy, as given by the Pauli principle. The second term is the attractive electro-

**Table 6** Ionization potential (IP), electron affinity (EA) and chemical hardness (η)

| $[Au_3Cl_3M_2]$ | IP (eV) | EA (eV) | η (eV) |
|---|---|---|---|
| Li | 10.20 | 1.29 | 4.45 |
| Na | 9.50 | 1.21 | 4.14 |
| K | 8.74 | 0.63 | 4.06 |
| Rb | 8.48 | 0.53 | 3.98 |
| Cs | 8.23 | 0.38 | 3.92 |

**Table 7** Fukui indices of electrophilic ($f^-$) and nucleophilic attack ($f^+$)

| $[Au_3Cl_3M_2]$ ($f^-$) | | | | | |
|---|---|---|---|---|---|
| Atom | Li | Na | K | Rb | Cs |
| Au | 0.17 | 0.19 | 0.33 | 0.34 | 0.34 |
| Cl | 0.16 | 0.12 | −0.01 | −0.01 | −0.01 |
| M | 0.05 | 0.03 | 0.02 | 0.01 | 0.01 |
| $[Au_3Cl_3M_2]$ ($f^+$) | | | | | |
| Au | −0.06 | −0.05 | −0.04 | −0.03 | −0.02 |
| Cl | 0.06 | 0.05 | 0.04 | 0.02 | 0.01 |
| M | 0.51 | 0.51 | 0.50 | 0.51 | 0.51 |

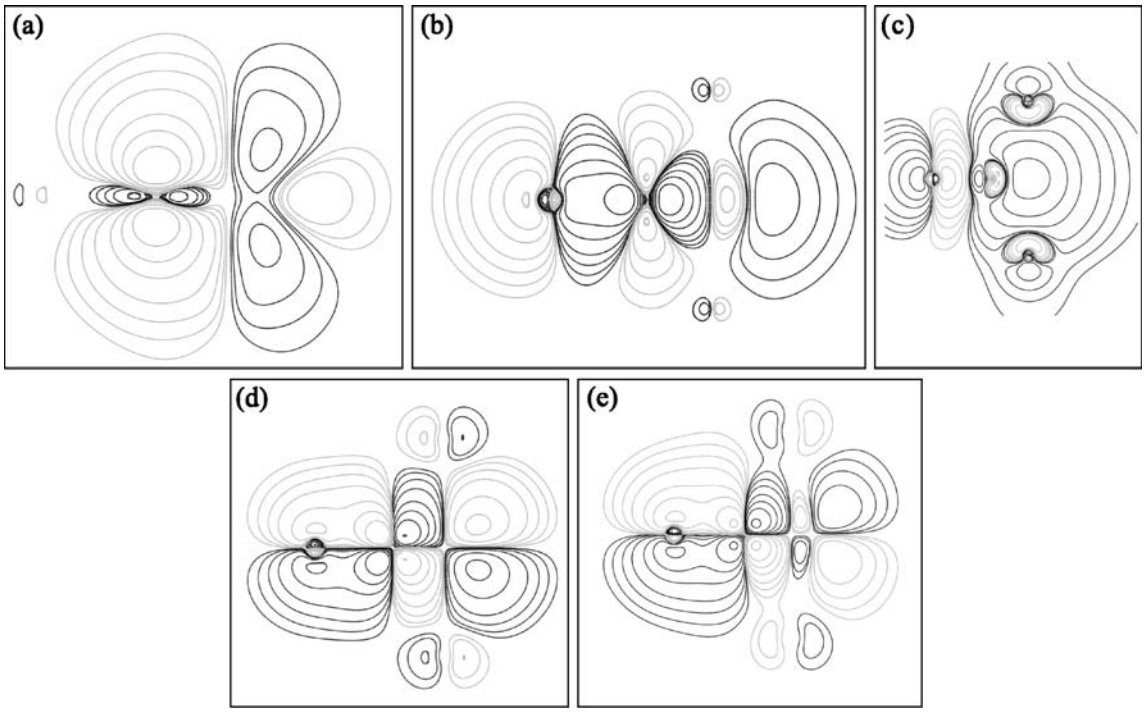


**Fig. 3** Contour plots of the main MOs involved in the back-donation interactions (the *slices* are in the plane perpendicular to the Au ring), **a** $[Au_3Cl_3Li_2]$ HOMO-12, **b** $[Au_3Cl_3Na_2]$ HOMO-16, **c** $[Au_3Cl_3K_2]$ HOMO, **d** $[Au_3Cl_3Rb_2]$ HOMO-20, **e** $[Au_3Cl_3Cs_2]$ HOMO-23

static overlap interaction ($E_{elec}$); summing over $E_{Pauli}$ and $E_{elec}$ result in the steric energy contribution.

The $[Au_3Cl_3]^{-2}$ cluster and the $M^+$ cations are considered as individual fragments to calculate the first two contributions in the total bonding energy and, at this step, their corresponding MOs are kept with no change. The third contribution, the orbital relaxation energy, is obtained by mixing the occupied and virtual MOs of the $[Au_3Cl_3]^{-2}$ and $2M^+$ fragments. In this term, the charge transfer and polarization contribution are important, since the charge transfer is the electronic population given from the occupied orbitals of one fragment to the unoccupied orbitals of the other fragment. On the other hand, in the polarization contribution, the transfer takes place from the occupied orbitals of the fragment to its own unoccupied orbitals. The partitioning of the bonding energy in the series of compounds is shown in Table 8. The electrostatic attraction energy is the main contribution to the total bonding energy in each of the species of the series, as stated above; while the orbital energy contributes only a small amount, which is consistent with the CDA results. Moreover, the electrostatic energies in the series represent, on average, 90% of the total bonding energies, which can be attributed to an ionic interaction between the $[Au_3Cl_3]^{-2}$ fragment and the $M^+$ alkaline cations. The large total bonding energies (ranging from −13 to −17 eV) computed from this methodology, suggest the considerable stability of the proposed complexes.

## Aromaticity

Like in the analogous $[Au_3Cl_3Tr_2]^{2+}$ compound [4], ring gold clusters have been shown to possess a strong aromatic character [13]. Magnetic shielding calculations using the

**Table 8** Bond energy partitioning for the series of complexes with zero-order relativistic approximation (ZORA) methodology at the Xα level

| Energy decomposition | ZORA | | | | |
|---|---|---|---|---|---|
| Energy contribution | eV | | | | |
| | $[Au_3Cl_3Li_2]$ | $[Au_3Cl_3Na_2]$ | $[Au_3Cl_3K_2]$ | $[Au_3Cl_3Rb_2]$ | $[Au_3Cl_3Cs_2]$ |
| Pauli repulsion energy (1) | +1.13 | +0.85 | +0.67 | +0.69 | +0.69 |
| Electrostatic attraction | −15.14 | −14.33 | −13.12 | −12.82 | −12.43 |
| Steric energy | −14.01 | −13.48 | −12.45 | −12.13 | −11.74 |
| Orbital relaxation (2) | −3.12 | −1.83 | −1.29 | −1.18 | −1.17 |
| Total bonding energy | −17.13 | −15.31 | −13.74 | −13.31 | −12.91 |

**Table 9** Nuclear independent chemical shift (NICS) calculations carried out at the B3LYP level of theory

| Complex | Computational method B3LYP NICS (ppm) |
|---|---|
| $[Au_3Cl_3Li_2]$ | −26.58 |
| $[Au_3Cl_3Na_2]$ | −25.05 |
| $[Au_3Cl_3K_2]$ | −24.15 |
| $[Au_3Cl_3Rb_2]$ | −37.02 |
| $[Au_3Cl_3Cs_2]$ | −23.76 |

NICS approach developed by Schleyer et al. [30] were carried out on the series; the results are shown in Table 9. A ghost atom was located at the geometrical center of the ring to determine the aromatic character in the metal monolayer sheet. A negative value of NICS is considered aromatic; a positive value antiaromatic; and a value close to zero, non-aromatic. As seen from Table 9, all molecules have a strong aromatic character, with a maximum at $[Au_3Cl_3Rb_2]$. These NICS values are comparable to those found in the $[Au_3Cl_3Tr_2]^{2+}$ compound [4].

The strong aromatic behavior observed on the $[Au_3Cl_3Rb_2]$ cluster reported by the higher NICS value may be due to the large d orbital population present on the plane of the ring and allocated on the lower energy orbitals (this population is significantly smaller in the rest of the species in the series) such as HOMO-4 through HOMO-6; these MOs are depicted in Fig. 2b. Therefore, the excess of d-electrons on the $Au_3$ ring would participate in the anomalous strengthening of the diatropic current addressed to the $Au_3Cl_3Rb_2$ cluster. The enhanced d orbital population present in this species may be due to Au–Au bonding on the ring, which is one of the shortest in the series. This special geometry gives rise to a stronger overlapping among d orbitals of gold on the plane of the $[Au_3Cl_3]^{-2}$ complex, triggering a larger density of electrons to the center of the ring.

The results for the rest of the species range from −26.58 to −23.76 ppm; such values are even higher than the NICS found for systems containing coinage metals. For instance, a value of −18.65 ppm has been reported for the $[Au_4Li_2]$ system, while a value of −26.58 ppm was found for $[Au_3Cl_3Li_2]$ in this work. Due to the large d-orbital character coming from lower molecular orbitals such as HOMO-1 through HOMO-3 (see Fig. 2a), a considerable d-electron delocalization is present and a δ-aromaticity would be expected. Consequently, the series of complexes $[Au_3Cl_3M_2]$ would be part of a limited group of species where delocalized d-electrons are mainly responsible for the occurrence of a new strong aromaticity. The aromatic character calculated by the NICS methodology is another indicator of the chemical stability in the series.

## Conclusions

The bonding trends along the series $[Au_3Cl_3M_2]$ (M = Li, Na, K, Rb, Cs) were studied by ab initio methods. A strong intermetallic interaction is evident in the central $Au_3$ ring. Evidence for both dispersion effects and covalent contributions is presented. According to the chemical hardness results, the stability in the series increases as the alkali metal becomes lighter, reaching its greatest value on the $[Au_3Cl_3Li_2]$ compound. The Au–Au bond lengths show a minimum at the most electropositive counterion, Cs. From the Fukui index criterion, it was shown that the Au atoms are the most probable sites in the molecules of the series where reactive activity may play a role. All the compounds of the series show an unusually strong aromatic character, as revealed by the NICS method. The delocalized d-electrons in the $Au_3$ ring are mainly responsible for the aromaticity observed in the series of complexes. A possible generalization of the present structures is an infinite, one dimensional chain ...–M–A–M–A–... where A is the present $[Au_3Cl_3]$ group and M, a divalent metal atom such as an alkaline earth.

**Acknowledgments** The authors wish to thank the IMPULSA Project (Investigación Multidisciplinaria de Proyectos Universitarios de Liderazgo y Superación Académica), PUNTA (Proyecto Universitario de Nanotecnología Ambiental); DGSCA-UNAM (Dirección General de Servicios de Cómputo Académico, Universidad Nacional Autónoma de México) and Instituto Potosino de Investigación Científica y Tecnológica (IPICYT) for providing computing time. J. M. acknowledges the support from Instituto de Investigaciones en Materiales (IIM-UNAM) under Project No. PAPIIT-IN107807. We also thank Prof. D. Sundholm for helpful discussion. P.P. belongs to the Finnish CoE in Computational Molecular Science.

## References

1. Murahashi T, Fujimoto M, Oka M, Hashimoto Y, Uemura T, Tatsumi Y, Nakao Y, Ikeda A, Sakaki S, Kurosawa H (2006) Science 313:1104–1107
2. Kurikawa T, Takeda H, Hirano M, Judai K, Arita T, Nagao S, Nakajima A, Kaya K (1999) Organometallics 18:1430–1438
3. Burdett JK, Canadell E (1985) Organometallics 4:805–815
4. Muñiz J, Sansores LE, Martínez A, Salcedo R (2008) J Mol Model 14:417–425
5. Schmidbaur H (1990) Gold Bull 23:11–21
6. Pyykkö P (2004) Angew Chem Int Ed 43:4412–4456
7. Schmidbaur H (1995) Chem Soc Rev 24:391–400
8. Mingos DMP (1996) J Chem Soc, Dalton Trans 5:561–566
9. van Zyl WE, López-de-Luzuriaga JM, Fackler JP Jr (2000) J Mol Struct 516:99–106
10. Pyykkö P (1997) Chem Rev 97:597–636
11. Tsipis AC, Tsipis CA (2003) J Am Chem Soc 125:1136–1137
12. Tsipis CA, Karagiannis EE, Kladou PF, Tsipis AC (2004) J Am Chem Soc 126:12916–12929
13. Wannere CS, Corminboeuf C, Wang Z-X, Wodrich MD, King RB, Schleyer PvR (2005) J Am Chem Soc 127:5701–5705

14. Lin Y-C, Sundholm D, Jusélius J, Cui L-F, Li X, Zhai H-J, Wang L-S (2006) J Phys Chem A 110:4244–4250
15. Møller C, Plesset MS (1934) Phys Rev 46:618–622
16. Andrae D, Haeussermann U, Dolg M, Stoll H, Preuss H (1990) Theor Chim Acta 77:123–141
17. Schäfer A, Huber C, Ahlrichs RJ (1994) J Chem Phys 100:5829–5835
18. Pyykkö P, Runeberg N, Mendizabal F (1997) Chem Eur J 3:1451–1457
19. Petersson GA, Al-Laham MA (1991) J Chem Phys 94:6081–6090
20. Petersson GA, Bennett A, Tensfeldt TG, Al-Laham MA, Shirley WA, Mantzaris J (1988) J Chem Phys 89:2193–2218
21. Hay PJ, Wadt WR (1985) J Chem Phys 82:299–310
22. Ziegler T, Rauk A (1977) Theor Chim Acta 46:1–10
23. Ziegler T, Rauk A, Baerends EJ (1977) Theor Chim Acta 43:261–271
24. Slater JC (1951) Phys Rev 81:385–390
25. Schwarz K (1972) Phys Rev B 5:2466–2468
26. Te Velde G, Bickelhaupt FM, Baerends EJ, Guerra CF, Van Gisbergen SJA, Snijders JG, Ziegler T (2001) J Comput Chem 22:931–967
27. Van Lenthe E, Baerends EJ, Snijders JG (1994) J Chem Phys 101:9783–9792
28. Van Lenthe E (1996) Int J Quantum Chem 57:281–293
29. van Lenthe E, Ehlers AE, Baerends EJ (1999) J Chem Phys 110:8943–8953
30. Schleyer PvR, Maerker C, Dransfeld A, Jiao H, Hommes NJvE (1996) J Am Chem Soc 118:6317–6318
31. Ghosh SK, Berkowitz M (1985) J Chem Phys 83:2976–2983
32. Berkowitz M, Ghosh SK, Parr RG (1985) J Am Chem Soc 107:6811–6814
33. Geerlings P, De Proft F, Langenaeker W (2003) Chem Rev 103:1793–1874
34. Yang W, Mortier WJ (1986) J Am Chem Soc 108:5708–5711
35. Gaussian 03, Revision D.01, Frisch MJ, Trucks GW, Schlegel HB, Scuseria GE, Robb MA, Cheeseman JR, Montgomery JA, Vreven T Jr, Kudin KN, Burant JC, Millam M, Iyengar SS, Tomasi J, Barone V, Mennucci B, Cossi M, Scalmani G, Rega N, Petersson GA, Nakatsuji H, Hada M, Ehara M, Toyota K, Fukuda R, Hasegawa J, Ishida M, Nakajima T, Honda Y, Kitao O, Nakai H, Klene M, Li X, Knox JE, Hratchian HP, Cross JB, Adamo C, Jaramillo J, Gomperts R, Stratmann RE, Yazyev O, Austin J, Cammi R, Pomelli C, Ochterski JW, Ayala PY, Morokuma K, Voth GA, Salvador P, Dannenberg JJ, Zakrzewski VG, Dapprich S, Daniels D, Strain MC, Farkas O, Malick DK, Rabuck D, Raghavachari K, Foresman JB, Ortiz JV, Cui Q, Baboul G, Clifford S, Cioslowski J, Stefanov BB, Liu G, Liashenko A, Piskorz P, Komaromi I, Martin RL, Fox DJ, Keith T, Al-Laham MA, Peng CY, Nanayakkara A, Challacombe M, Gill PMW, Johnson B, Chen W, Wong MW, Gonzalez C, Pople JA (2004) Gaussian Inc, Wallingford CT
36. Fonseca-Guerra C, Snijders JG, Te Velde G, Baerends EJ (1998) Theor Chem Acc 99:391–403
37. ADF2006.01, SCM, Theoretical Chemistry, Vrije Universiteit, Amsterdam, The Netherlands, http://www.scm.com
38. Bravo-Pérez G, Garzón IL, Novaro O (1999) J Mol Struct (Theochem) 493:225–231
39. Muñiz J, Sansores LE, Martínez A, Salcedo R (2007) J Mol Struct (Theochem) 820:141–147
40. Parr RG, Pearson RG (1983) J Am Chem Soc 105:7512–7516
41. Pearson RG (1987) J Chem Ed 64:561–567
42. Parr RG, Chattaraj PK (1991) J Am Chem Soc 113:1854–1855
43. Gázquez JL (1993) In: Sen KD (ed) Hardness, series structure, bonding, vol 80. Springer, Berlin, p 27
44. Parr RG, Gázquez JL (1993) J Phys Chem 97:3939–3940
45. NBO Version 3.1, Glendening ED, Reed AE, Carpenter JE, Weinhold F (included in the GAUSSIAN 03 package of programs)
46. Wu X, Senapati L, Nayak K, Selloni A, Hajaligol M (2002) J Chem Phys 117:4010–4015
47. Fielicke A, von Helden G, Meijer G, Simard B, Rayner DM (2005) Phys Chem Chem Phys 7:3906–3909
48. Hashmi ASK, Hutchings G (2006) Angew Chem Int Ed 45:7896–7936
49. Schwerdtfeger P (2003) Angew Chem Int Ed 42:1892–1895
50. Dapprich S, Frenking G (1995) J Phys Chem 99:9352–9362